IEEE Access
Multidisciplinary | Rapid Review | Open Access Journal

Received July 17, 2019, accepted July 27, 2019, date of publication July 31, 2019, date of current version August 14, 2019.

Digital Object Identifier 10.1109/ACCESS.2019.2932180

EEG Control of a Bionic Hand With Imagination Based on Chaotic Approximation of Largest Lyapunov Exponent: A Single Trial BCI Application Study

AMIN HEKMATMANESH, REZA MOHAMMADI ASL, HUAPENG WU, AND HEIKKI HANDROOS, (Member, IEEE)
Laboratory of Intelligent Machines, Department of Mechanical Engineering, LUT University, FI-53850 Lappeenranta, Finland
Corresponding author: Amin Hekmatmanesh (amin.hekmatmanesh@lut.fi)

ABSTRACT This paper investigates a method for imaginary hand fisting pattern recognition based on the electroencephalography (EEG). The proposed method estimate the largest Lyapunov exponent (LLE) chaotic feature that is based on approximation of mutual information (MI) and false nearest neighbor (FNN) methods for reconstructing a phase space. The selected method for MI and FNN approximation approaches is a new version of Tug of War optimization algorithm. The new algorithm utilizes chaotic maps to update candidate solutions. The chaotic approximation of the LLE (CALLE) is the utilized method for extracting the chaotic features and then categorizing features by means of soft margin support vector machine with a generalized radial basis function kernel classifier. Accuracy and paired t-test values are obtained and compared with the traditional LLE method; 18 candidates were participated to record the EEG for imaginary right-hand fisting task. The results show improvements for the CALLE algorithm in comparison with the traditional LLE by achieving a higher accuracy of 68.25%. Feature changes between two imaginary statuses were significant for 17 subjects, and the paired t-test values were ($p < 0.05$). From the results, it is concluded that the Tug of War optimization method finds different values to reach a higher accuracy than the traditional LLE method, and the traditional methods for the LLE are not optimum.

INDEX TERMS Chaos optimization, largest Lyapunov exponent (LLE), mutual information, false nearest neighbor (FNN), Tug of War optimization.

I. INTRODUCTION

Brain computer interface (BCI) based on electroencephalography (EEG) signal processing is one of the methods for assisting paralyzed patients for a convenient life. For this purpose, different methods are developed to diagnose the patients thinking of fisting through the EEG signals. Some well-known methods are the common spatial pattern (CSP) [1], [2], wavelet [3], [4], fractal dimensions [5], [6] and chaotic features [7]. Chaos theory has been used to predict nonlinear system's behavior such as EEG signals. In the chaotic computations, initial values are significant to avoid instability of nonlinear systems. To investigate the chaotic behavior of systems, quantifiers are employed, such as fractal dimensions and Largest Lyapunov Exponent (LLE) [8]. One prominent chaotic quantifier is the LLE, which is based on reconstructing system's trajectory in a phase space. The LLE is a successful method for detecting different EEG patterns, such as epilepsy [9], spindle patterns [8] and ADHD [10]. For instance, Allahverdy *et al.* [11] used a set of chaotic features such as the LLE, Higuchi fractal dimension (FD), Sevcik FD and Katz FD to diagnose the ADHD patterns in the EEG signals. In a recent study, Korda *et al.* [12] used the LLE features for detecting eye movement patterns automatically. Moreover, Dahat *et al.* [13] utilized the LLE feature to investigate the chaotic brain's behavior in sleep stages. In this study, the LLE will be used to diagnose the two imaginary status of right hand fisting imagination and no fisting imagination. The initial values for the traditional LLE will be optimized by artificial intelligence (AI) methods.

The associate editor coordinating the review of this manuscript and approving it for publication was Ludovico Minati.

On the other hand, the usage of the different methods of the AI, neural networks [14], fuzzy logic [15] and evolutionary algorithms [16] has been increased in recent years. For instance, a type-2 fuzzy system has been used for signal classification. The fuzzy logic based approach has been used to classify the EEG signals [17]. In another research, a neural network based method has been investigated for different purposes. The method has been developed in a way that, the neural network has been used for learning, classification, and comparative analysis of brain data [18]. Evolutionary algorithms are one of the most strong methods of the AI. These algorithms are widely used to solve engineering problems [19]. For example, particle swarm optimization algorithm has been employed to optimize a neural network weights [20]. The optimized one has been used to detect and extract features from the EEG signals. In [21], a binary flower pollination algorithm has been used to identify persons based on EEG signals. The method has been developed for sensor selection in the EEG signals. The Tug of War Optimization has been introduced recently by Kaveh [22]. The algorithm has been used to solve different engineering problems. For instance, it has been used to optimize the design of castellated beams [23]. Considering its results of its applying on different benchmark optimization problems, however it can be supposed as one of strong new optimization methods, new improvements can be applied on the basic algorithm to enhance its performance.

In this study, our contribution is reconstructing two phase spaces based on the traditional LLE and Chaotic Approximation LLE (CALLE) and drawing the trajectory of the EEG to diagnose right hand fisting imagination and no fisting imagination status. For reconstructing the phase space, mutual information (MI) and false nearest neighbor (FNN) approaches are computed. Thereafter, the approximated phase space is reconstructed based on the AI method as substitute of traditional delay for the MI and embedding dimension for the FNN. The new developed chaotic tug of war optimization (CTWO) algorithm is selected as the AI method. The new developed algorithm uses chaotic maps to update the candidate solutions. The LLE feature is extracted from the trajectories of the right hand fisting imagination and no fisting imagination status in the phase spaces. To classify the CALLE features of the status in the reconstructed phase spaces, the Soft Margin Support Vector Machine (SMSVM) with the Generalized Radial Basis Function (GRBF) is utilized.

II. METHODS & MATERIALS

Regarding the Taken's theory [24] for computing the CALLE, the phase space is first reconstructed using the MI and FNN methods, and then the MI and FNN are computed traditionally. Next, the MI (lag parameter) and FNN (embedding dimension) values are updated by the Tug of War approach. The reconstructed phase spaces are employed for extracting the traditional LLE and CALLE features, and also considering the trajectory differences. As the first step the MI approach is implemented as follows:

A. PRE-PROCESSING

In order to prepare the signal for processing, pre-processing procedures are applied. The raw EEG signal is first segmented from 200 ms before displaying pictures to 2500 ms after displaying pictures. The segmented signals are then passed through a six order Butterworth filter with 8-15 Hz edges [4]. Finally the filtered signal is normalized between zero and one for the further processing.

B. MUTUAL INFORMATION (MI)

One of the principals of the phase space reconstruction is computing an optimum time lag (ζ), which is obtained through the MI approach [11]. The MI required two input values, signal and maximum delay as a function criterion, which is selected $max\zeta = 10$ as a constant value. Then, the MI is utilized to extract information between two intervals of x_t and $x_{t+\zeta}$. The MI is a method to compute the ζ parameter as follows:

$$MI(\zeta) = \sum_{i=1}^{j}\sum_{s=1}^{j} Pr_{i,s}(\zeta)\log_2\left(\frac{Pr_{i,s}(\zeta)}{Pr_i Pr_s}\right), \tag{1}$$

where, i and s are the interval indexes for x_t, $x_{t+\zeta}$, respectively. Also, Pr_i and Pr_s are existing probabilities of the x_t value in the $i-th$ and the $s-th$, respectively. The second step for computing the LLE is computing the FNN algorithm as follows:

C. FALSE NEAREST NEIGHBOR (FNN)

The second important parameter for reconstructing a phase space is estimating the embedded dimension (n). The FNN algorithm required signal and maximum embedding dimension criterion as inputs, which is selected three based on the traditional computations. Each phase space's dimension is computed by $x_j = x_s, x_{s+\zeta}, x_{s+2\zeta}, ..., x_{s+(n-1)\zeta}, s = 1, ..., N$. The proper value for n-dimension is obtained by the FNN approach. Two delayed of the EEG signal is used to reconstruct the signal attractor with assumption of no intersection in the reconstructed phase space based on the MI and FNN. Attractors are trajectory of a system that tends to grow. If an intersection occur, the phase space dimension will be increased since no intersection is counted. Therefore, the number of intersections are the FNN value that is utilized for increasing the phase space dimension [25]. For computing the LLE, the MI and FNN parameters are determined and the LLE is computed as follows:

D. LARGEST LYAPUNOV EXPONENT (LLE)

For each input segments, the average value of exponential divergence along the grew trajectory will be computed and called the Lyapunov Exponent (LE). To compute the LLE (γ), the FNN and MI parameters are used as inputs for constructing the phase space. Next, through $Q(t) = Ee^{\gamma t}$ divergence of the grew trajectory is applied on pair neighbor

trajectories at time t and initial separation E. The Logarithmic distance $Q_j(m)$ is computed between the pair of neighbors by $\ln(Q_j(m)) \approx \gamma(m.\Delta t) + \ln(E_j)$, where m is the counter for the pairs [26], [27]. Finally, the maximum exponential slopes for each segment is called the LE and obtained as follows [25]:

$$LE(i) = \frac{1}{\Delta t} \times \frac{1}{j} \sum_{1}^{j} \ln[Q_j(i)]. \tag{2}$$

The computed LLE (γ) has following conditions:
1- $\gamma > 0$ indicates chaotic;
2- $\gamma = 0$ indicates limit cycle;
3- $\gamma < 0$ indicates stable behavior.

The largest *LE* for each segment is the LLE. Then, the LLE values are then classified by the SMSVM classifier with the GRBF kernel. In the traditional LLE, the MI and FNN algorithms have two constant values that are obtained experimentally. In the next section, the delay and embedding dimension parameters in the MI and FNN methods in the CALLE algorithm is updated by the CTWO algorithm.

E. CHAOTIC TUG OF WAR OPTIMIZATION (CTWO)

The Tug of war optimization algorithm has been introduced recently by Kaveh [23]. The algorithm has been built on the concept of Tug of War between two groups. The author has developed the physical principal on the groups and the interaction between them. Considering these principles, the Tug of War Optimization has been developed as following steps:

Step 1 Initialization: The initial population is generated as following:

$$X_i^0 = L_B + rand * (U_B - L_B), \quad i = 1, \ldots, N \tag{3}$$

where X_i^0 is the initial value of the ith candidate solution, and N is the number of candidates. The upper and lower bound of the search space are shown by U_B, and L_B, respectively.

Step 2 Weight assignment: Each candidate solution is supposed as a team in the competition, and it is needed that the weight of each candidate is calculated in comparison between others. The weight of each one can be calculated as following:

$$W_i = \frac{F_i - F_{worst}}{F_{best} - F_{worst}} + 1, \quad i = 1, \ldots, N \tag{4}$$

where W_i is the weight of ith team, and its fitness value is shown by F_i. At current iteration, the best and worst value of the fitness function between population are given by F_{best}, and F_{worst}, respectively.

Step 3 Competition and displacement: Each candidate team has a displacement after competing with each other team. The displacement can be given as following equation:

$$\Delta X_i = \sum_{j=1}^{N} \Delta X_{ij},$$
$$\Delta X_{ij} = \frac{1}{2} a_{ij} \Delta t^2 + \alpha\beta \, (U_B - L_B) * rand, \tag{5}$$

where ΔX_{ij} is the displacement of the ith candidate, and ΔX_{ij} is the displacement of the ith candidate in competition with the jth candidate. The parameter α is proportional factor, and β is a factor between (0, 1]. The parameter a_{ij} is the acceleration of the ith candidate in comparison with the jth candidate, and can be computed as following:

$$a_{ij} = g_{ij} * \frac{F_{r,ij}}{W_i \mu},$$
$$g_{ij} = X_j - X_i,$$
$$F_{r,ij} = F_{p,ij} - W_i \mu, \tag{6}$$

where g_{ij} is gravitational acceleration constant, and $F_{r,ij}$ is resultant force affecting factor. The pulling force between ith and jth teams is given by $F_{p,ij}$, and is the maximum of two values ($W_i\mu$, $W_j\mu$).

Step 4 New generation: The new candidates is computed by following formula:

$$X_i^{new} = X_i^{old} + \Delta X_i. \tag{7}$$

Step 5 Termination: If any of stop criteria is reached, stop algorithm and return the best solution, else, go to step 2 [28].

The above mentioned steps, a random number has been used in equation (5). This random factor can be changed in a way that can consider the fitness value of the candidate solution to update it. Let suppose that a chaotic map is chosen to calculate the factor regarding to the value of the fitness function. By considering this definition, the equation (5) can be expressed as following:

$$\Delta X_{ij} = \frac{1}{2} a_{ij} \Delta t^2 + \xi_{ij} * (U_B - L_B), \tag{8}$$

where ξ_{ij} is the chaotic factor and it is calculated as

$$\xi_{ij} = \Xi \left(F_i - F_j \right),$$

where the chaotic map is shown by function Ξ. The definition and well-known chaotic maps are reviewed in the following section.

1) CHAOTIC MAPS

One of the well-known random based methods, which is used in solving optimization problems, is chaotic optimization algorithms. These algorithms use chaotic variables. Unlike stochastic searches, which are based on probabilities, chaos is based on two features: the non-repetition and the ergodicity. Therefore, it has higher full search speed than stochastic searches. Chaos applies 12 one-dimensional non-invertible maps and generates chaotic sets as shown in Table 1. These sets are used to achieve chaos goal, which is providing high full search speed. For more information about COA method and 12 chaotic maps readers can refer to [29].

TABLE 1. Chaotic maps.

Number	Name	Definition
M_1	Chebyshev map	$x_{k+1} = \cos(k \cos^{-1}(x_k))$
M_2	Circle map	$x_{k+1} = x_k + b - (\frac{a}{2\pi}) \sin(2\pi k) \mod 1$
M_3	Iterative map	$x_{k+1} = \sin(\frac{a\pi}{x_k}), a \in (0, 1)$
M_4	Logistic map	$x_{k+1} = a x_k (1 - x_k)$
M_5	Sine map	$x_{k+1} = \frac{a}{4} \sin(\pi x_k), \quad 0 < a \leq 4$
M_6	Singer map	$x_{k+1} = \mu(7.86x_k - 23.31x_k^2 + 28.75x_k^3 - 13.302875x_k^4)$
M_7	Sinusoidal map	$x_{k+1} = a x_k^2 \sin(\pi x_k)$
M_8	Tent map	$x_{k+1} = \begin{cases} \frac{x_k}{0.7} & x_k < 0.7 \\ \frac{10}{3}(1 - x_k) & x_k \geq 0.7 \end{cases}$
M_9	Gaussian map	$x_{k+1} = \begin{cases} 0 & x_k = 0 \\ \frac{1}{x_k} \mod 1 & otherwise \end{cases}, \frac{1}{x_k} \mod 1 = \frac{1}{x_k} - [\frac{1}{x_k}]$
M_{10}	Intermittency map	$x_{k+1} = \begin{cases} \varepsilon + x_k + c x_k^n & 0 < x_k \leq P \\ \frac{x_k - P}{1 - P} & P < x_k < 1 \end{cases}$
M_{11}	Liebovitch map	$x_{k+1} = \begin{cases} \alpha x_k & 0 < x_k \leq P, \\ \frac{P - x_k}{P_2 - P_1} & P_1 < x_k \leq P_2, \\ 1 - \beta(1 - x_k) & P_2 < x_k \leq 1 \end{cases}$
M_{12}	Piecewise map	$x_{k+1} = \begin{cases} \frac{x_k}{P} & 0 \leq x_k < P \\ \frac{x_k - P}{0.5 - P} & P \leq x_k < \frac{1}{2} \\ \frac{1 - P - x_k}{0.5 - P} & \frac{1}{2} \leq x_k < 1 - P \\ \frac{1 - x_k}{P} & 1 - P \leq x_k < 1 \end{cases}$

TABLE 2. The detail of benchmark functions.

Number	Function	Formulation	D	Minimum
F_1	Beale	$f(x) = (1.5 - x_1 + x_1 x_2)^2 + (2.25 - x_1 + x_1 x_2)^2 + (2.625 - x_1 + x_1 x_2)^2$	2	0
F_2	Bohachevsky 1	$f(x) = x_1^2 + 2x_2^2 - 0.3\cos(3\pi x_1) - 0.4\cos(4\pi x_2) + 0.7$	2	0
F_3	Bohachevsky 2	$f(x) = x_1^2 + 2x_2^2 - 0.3\cos(3\pi x_1)(4\pi x_2) + 0.3$	2	0
F_4	Bohachevsky 3	$f(x) = x_1^2 + 2x_2^2 - 0.3\cos(3\pi x_1 + 4\pi x_2) + 0.3$	2	0
F_5	Booth	$f(x) = (x_1 + 2x_2 - 7)^2 + (2x_1 + x_2 - 5)^2$	2	0
F_6	Achley	$f(x) = -20\exp\left(-0.2\sqrt{\frac{1}{n}\sum_{i=1}^{D} x_i^2}\right) - \exp\left(\frac{1}{n}\sum_{i=1}^{D}\cos(2\pi x_i)\right) + 20 + e$	30	0
F_7	Schwefel 2.22	$f(x) = \sum_{i=1}^{D} \lvert x_i \rvert + \Pi_{i=1}^{D} \lvert x_i \rvert$	30	0
F_8	Rosenbrock	$f(x) = \sum_{i=1}^{D-1} 100\left(x_{i+1} - x_i^2\right)^2 + (x_i - 1)^2$	30	0
F_9	Rastrigin	$f(x) = \sum_{i=1}^{D}\left(x_i^2 - 10\cos(2\pi x_i) + 10\right)$	30	0
F_{10}	Griewank	$f(x) = \frac{1}{4000}\left(\sum_{i=1}^{D}(x_i - 100)^2\right) - \left(\Pi_{i=1}^{D}\cos\left(\frac{x_i - 100}{\sqrt{i}}\right)\right) + 1$	30	0

2) CTWO VALIDATION

This section compares the performance of the CTWO with different chaotic maps to the performance of Tug of War Optimization using 10 benchmark functions. The new designed algorithm is applied on different kind of benchmark functions. The functions can be divided into two generic groups: separable and non-separable. The mathematical formula and details of these functions are presented in Table 2. In order to have the same condition for the comparison between different algorithms, reaching to the maximum number of evaluation of the cost function is supposed as stop criteria. The maximum number is set on 10000. In the report about the comparison, any value less than 10^{-10}, is considered as zero. The result of the application of the CTWO on different benchmark functions with different chaotic maps, which is indicated by M_i, are presented in Table 3. The performance of the proposed algorithm are compared with the result of traditional algorithms, genetic algorithm (GA), particle swarm

TABLE 3. Comparative results of CTWO with different chaotic map, TWO, GA, and PSO.

Alg. \ Func.	Chaotic Map	F_1	F_2	F_3	F_4	F_5	F_6	F_7	F_8	F_9	F_{10}
CTWO	M_1	0	0.0548	5.5E-06	0	0.0060	0.0642	4.8E-03	0.0742	0	8.8E-06
	M_2	0.0754	0	0.0597	0	7.5E-05	0.0694	0	6.4E-09	0.0030	0.0755
	M_3	0.878	4.8E-07	0.0070	0	0.0675	0	5.9E-08	0.0861	0.0732	0
	M_4	6.7E-09	0.0889	0.0046	0.0074	5.4E-06	0.0768	0.0819	0	0.0724	8.4E-05
	M_5	0	0.0778	0.0963	0.0043	7.6E-02	0.0716	6.6E-08	0	0.0073	0.0928
	M_6	4.4E-08	0.0744	0.0877	0.0048	0	7.7E-04	0.0766	0.0055	0.0433	6.2E-05
	M_7	0.0533	0	2.3E-01	0.0088	0.0812	0.0625	3.4E-05	0	0.716	0.0026
	M_8	6.9E-06	0.0466	0.0749	0	5.4E-03	8.9E-04	0.0032	0.0955	0.0043	6.7E-03
	M_9	0.0549	0.0645	0.0089	0	5.8E-06	0.0926	0.0025	4.4E-07	3.7E-04	0
	M_{10}	0.0866	6.1E-06	0.0755	0.0066	0	8.2E-06	0.0911	0.0028	0.0618	0
	M_{11}	0	4.5E-07	0.0743	0.0033	0.0621	5.1E-01	0.0477	0	6.2E-08	0.0027
	M_{12}	3.7E-04	0	0.0744	0.0053	0.0944	0	0.0046	8.7E-04	0.0655	0
TWO	-	0	8.8E-02	0.0744	0.0834	4.8E-04	0.0522	0.0046	0.0876	0.0051	6.4E-09
PSO	-	0.0499	0	2.6E-05	0.0621	3.7E-06	0.0082	0.0766	0	0.0839	7.3E-05
GA	-	0	7.2E-03	0.0974	0.0056	0	0.0566	8.1E-06	0.0814	0.0092	6.2E-03

optimization (PSO), and basic tug of war optimization (TWO) in the Table. The enhancement of the behavior of the basic algorithm and the verification of new algorithm as an optimization method can be drawn regarding the comparative results which are given. Based on the previously introduced method which are implemented to enhance the performance of evolutionary algorithm, there is not any specific method to select a specific chaotic map, which can have a global optimized results [30], [31]. Considering this fact and the comparative results in Table. 3, it is obvious that the chaotic map should be selected based on the experience of the designer and/or trial and error. The obtained optimized values for the delay and embedding dimension are then used to compute the LLE features. Next, the CALLE features are classified using the SMSVM classifier with the GRBF kernel, that is described as follows:

F. CLASSIFIER

The extracted LLE and CALLE features for the status imaginary hand fisting and no imagination are classified by the SMSVM with the GRBF kernel. The GRBF kernel computations are presented as follows:

1) GENERALIZED RADIAL BASIS FUNCTION

One effective modification of RBF is the GRBF, which is implemented by adding three free parameters of Ce, τ and We instead of the fixed values for center, shape and width of the Gaussian distribution function in Eq. 9, respectively. It is showed that the GRBF is flexible and reliable method that is described in Eqs. 9-11 [5], [6], [32]. Figs. 1a and 1b are the prof of the flexibility of the Generalized Gaussian Function (GGF) and it's effects in the GRBF for different 10 τ values

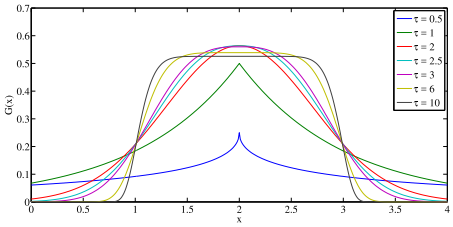

(a) 10 values of τ with two fixed points of $We = 1$ and $Ce = 2$ to show the GGF flexibility.

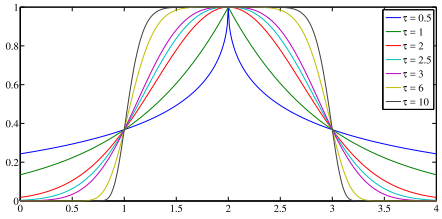

(b) 10 values of τ with two fixed points of $We = 1$ and $Ce = 2$ to show the GRBF flexibility.

FIGURE 1. Generalized Radial Basis Function.

with $c = 2$ and $W = 1$.

$$G(g; Ce, We, \tau) = \frac{\tau}{2We\psi(1/\tau)} \exp(-\frac{\|g - Ce\|}{We^{\tau}}), \quad (9)$$

ψ is a factorial extension, which is obtained by Eq. 10:

$$\psi(t) = \int_0^{\infty} l^{t-1} e^{-t} dt, \quad \text{for } l > 0. \quad (10)$$

The final weight We is computed by standard deviation (SD) in Eq. 10:

$$We = SD\sqrt{\frac{\psi(^1/_\tau)}{\psi(^3/_\tau)}}, \tag{11}$$

To classify the LLE and CALLE features, the GRBF function is used as a kernel of the SMSVM classifier algorithm as follows:

2) SOFT MARGIN SUPPORT VECTOR MACHINE (SMSVM)

SMSVM is a powerful method for classifying [33]. Based on the extracted LLE features, two label classes of $S = [-1, +1]$ and a training data set of $Y_i \in R^n, j = 1, ..., l$ are defined.

The utilized decision boundary in the SVM-based classifiers is $w^T z_i + C = 0$ with following criterion:

$$\begin{aligned} W^T Y_i + C \geq 1 \qquad & \text{if} \quad S_i = 1, \\ W^T Y_i + C \leq -1 \qquad & \text{if} \quad S_i = -1, \end{aligned} \tag{12}$$

where Y, W and C are the input values, achieved weights and bias, respectively. To find the best decision boundary a hyper plane is defined and adjusted between the two classes data set. The best location of the hyper plane is specified by some selected features called support vectors (SVs). exploring the hyperplane location is based on maximizing margin distance between the features of the two classes. The selected maximized features are named support vectors (SVs) that are computed using Eq. 13:

$$f(Y) = sgn(W^T Y + C). \tag{13}$$

In cases of nonlinear data set a nonlinear kernel of $\phi(Y_i)$ is defined. To this purpose, the $\phi(Y_i)$ is used as a transfer function to map the obtained features into higher dimension. By greatly increasing the number of features, feature space dimension is increased and duality problem is occurred. To solve the duality problem, a number of features are controlled using Lagrange's theorem, Eq. 14. Therefore, the decision boundary is modified to $W^T \phi(Y) + C = 0$ as follows [34]:

$$\begin{aligned} \min_{W,C,\alpha} \; & (\frac{1}{2} W^T W + Re \sum_{i=1}^{l} \alpha_i) \\ & Y_i(W^T \phi(Y_i) + C) \geq 1 - \alpha_i \\ \text{Subject to } & \alpha_i \geq 0 \\ & i = 1, ..., l, \end{aligned} \tag{14}$$

In order to control the cost of computations (α_i) in the training set of $(\alpha(W; Y, S) \equiv (1 - SW^T Y)^2)$ a regularized parameter Re is defined as follows:

$$\begin{aligned} \min_{\alpha} \; & (\frac{1}{2} \sum_{i,j=1}^{N} \alpha_i{}^T S_i S_j K(Y_i, Y_j) \alpha_j - \sum_{i=1}^{N} u^T \alpha_i) \\ & S^T \alpha = 0, \\ \text{Subject to } & 0 \leq \alpha_i \leq Re \\ & i = 1, ..., l, \end{aligned} \tag{15}$$

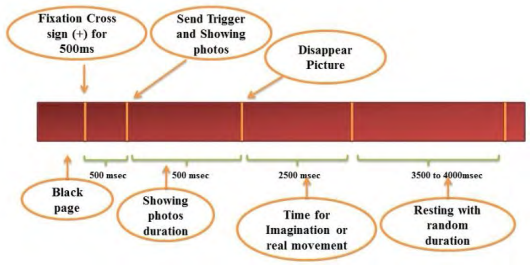

FIGURE 2. Designed task procedure based on the relative research [3].

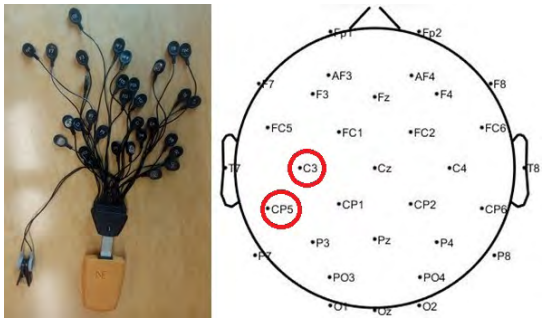

FIGURE 3. The utilized Enobio amplifier with 32 sensor locations.

FIGURE 4. Imaginary hand fisting experiment.

where u is unit matrix and α is the Lagrange obtained coefficients, respectively; and k is the selected kernel function in Eq. 15, $K(Y_i, Y_j) \equiv \phi(Y_i)^T \phi(Y_j)$. To find the best decision boundary in Eq. 15, the W must be optimized by $W = \sum_{i=1}^{l} S_i \alpha_i \phi(Y_i)$. The final hyper plane is applied using Eq. 16:

$$sgn(W^T \phi(Y) + C) = sgn(\sum_{i=1}^{l} S_i \alpha_i K(y_i, y) + C). \tag{16}$$

III. DATA ACQUISITION

18 subjects (S1-S18) with the average age of 29.5 years old are participated in the experiment. It was considered that participants did have history of addiction to alcohol and narcotic drugs. Also, it was considered that they did not use caffeinated materials at least four hours before test. To record the EEG data the same procedure is defined in [3]. In summary, the procedure has four steps in following order (Fig. 2): 1- a black screen with fixation cross at the center;

TABLE 4. Accuracy results of imaginary the hand fisting detection based on the CALLE feature. The estimated average dimensions and delays based on the CTWO method for the hand fisting imagination and no fisting imagination status are presented. The paired t-test between the two status for the CALLE features are computed.

Subjects	Dimension for fisting imagination	Delay for fisting imagination	Dimension for no imagination	Delay for no imagination	Offline Accuracy%	paired t-test
S1	45	14	32	11	56.66	$p > 0.05$
S2	48	55	36	96	66.00	$p < 0.05$
S3	52	55	48	24	70.00	$p < 0.05$
S4	44	38	6	78	66.00	$p < 0.05$
S5	24	81	25	43	70.00	$p < 0.05$
S6	47	52	19	21	70.00	$p < 0.05$
S7	45	77	33	20	67.33	$p < 0.05$
S8	9	90	42	7	67.33	$p < 0.05$
S9	6	45	14	31	70.00	$p < 0.05$
S10	38	22	38	19	64.67	$p < 0.05$
S11	33	11	3	5	64.65	$p < 0.05$
S12	18	13	35	56	64.33	$p < 0.05$
S13	36	2	19	74	75.00	$p < 0.05$
S14	7	49	37	47	70.00	$p < 0.05$
S15	25	97	19	37	65.00	$p < 0.05$
S16	14	63	2	81	70.00	$p < 0.05$
S17	13	40	33	86	70.00	$p < 0.05$
S18	30	70	30	81	70.00	$p < 0.05$
Average	-	-	-	-	68.25	-

TABLE 5. Accuracy results of imaginary hand fisting detection based on the traditional LLE features. The obtained average dimensions and delays based on the traditional methods for the right hand fisting imagination and no fisting imagination status are presented. The paired t-test between the two status for the LLE features are computed.

Subjects	Dimension for fisting imagination	Delay for fisting imagination	Dimension for no imagination	Delay for no imagination	Offline Accuracy	paired t-test
S1	2	5	2	5	50.00	$p > 0.05$
S2	1.96	30	1.96	30	55.00	$p > 0.05$
S3	2	25.6	2	25.5	60.00	$p < 0.05$
S4	1.94	30	1.94	30	55.00	$p > 0.05$
S5	2	5	2	5	60.00	$p < 0.05$
S6	2	5	2	5	60.00	$p < 0.05$
S7	2	5	2	5	50.00	$p > 0.05$
S8	2	5	2	5	60.00	$p < 0.05$
S9	2	5	2	5	60.00	$p < 0.05$
S10	2	5	2	5	55.00	$p > 0.05$
S11	2	5.6	2	6.3	55.00	$p > 0.05$
S12	2	5	2	5	50.00	$p > 0.05$
S13	2	5	2	5	60.00	$p < 0.05$
S14	2	5	2	5	60.00	$p < 0.05$
S15	2	5	2	5	65.00	$p < 0.05$
S16	2	5	2	5	65.00	$p < 0.05$
S17	2	5	2	5	60.00	$p < 0.05$
S18	2	5	2	5	60.00	$p < 0.05$
Average	-	-	-	-	57.77	-

2- displaying photos of hand fisting; 3- imagination of right hand fisting; 4- resting for three to four sec randomly. The pictures were sketch of a hand and a black page for no imagination. After displaying the sketch of the right hand, the subjects have to imagine the right hand fisting for 2500 msec; and displaying a black screen means no

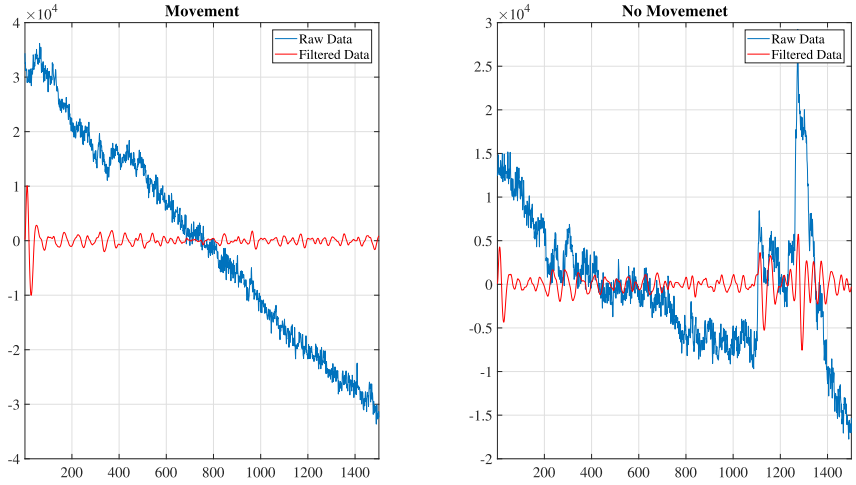

(a) Filtered EEG data for the imaginary fisting and no imagination status for the C3 channel. The imaginary fisting pattern is identified between 800-900 msec.

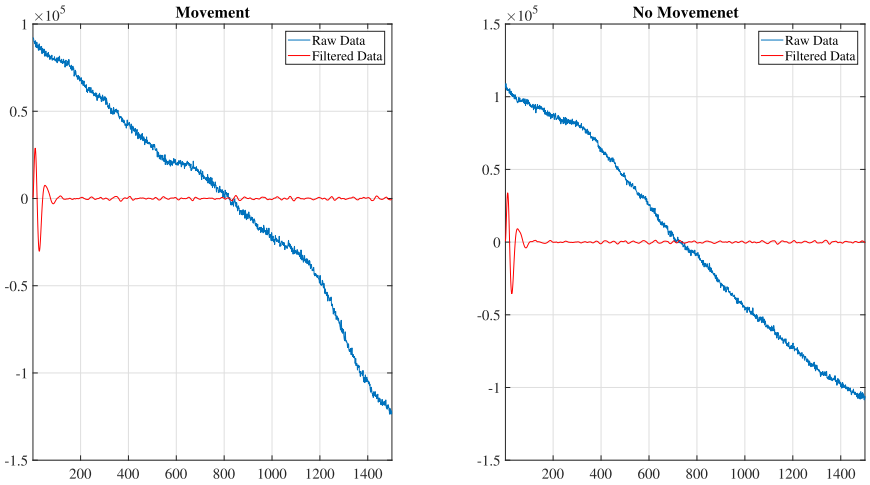

(b) Filtered EEG data for the imaginary fisting and no imagination status for the CP5 channel. The imaginary fisting pattern is identified between 800-900 msec.

FIGURE 5. **The Raw and filtered EEG data for the C3 and CP5 channels for the two status of imaginary fisting and no imagination.**

fisting imagination. This cycle is presented for 150 trials for offline processing and 20 trails for real-time processing. The system is synchronized with a bionic hand to investigate the speed and accuracy of the system in real-time mode, Fig.4. The data is recorded utilizing ENObio amplifier with 32 dry electrodes, Fig. 3. The frequency sampling of the ENObio amplifier is adjusted to 500 Hz.

IV. RESULTS

In the BCI experiment the EEG is recorded based on the presented procedure in Fig. 2. The CALLE features are classified with the SMSVM method that the obtained results are presented in Tables 4 and 5. The results are evaluated based on accuracy and paired t-test evaluations. To consider the properties of the reconstructed phase space and CALLE values, Figs. 6 and 7 for S13 are showed and discussed. The 32 EEG channels gives information of the neurons activity in 32 locations. More specifically, C3 (channel 15) and CP5 (channel 28) locations are the aim areas of generating imaginary movement patterns in this data set, Fig. 5 [3]. Trajectory of the mentioned channels for S13 are presented in the Figs. 8-10. Fig. 8 is the trajectory of the channels C3 and CP5 using traditional method for reconstructing the phase space. Figs. 9 and 10 are the trajectories in the estimated reconstructed phase space for the two different projections from the channels C3 and CP5.

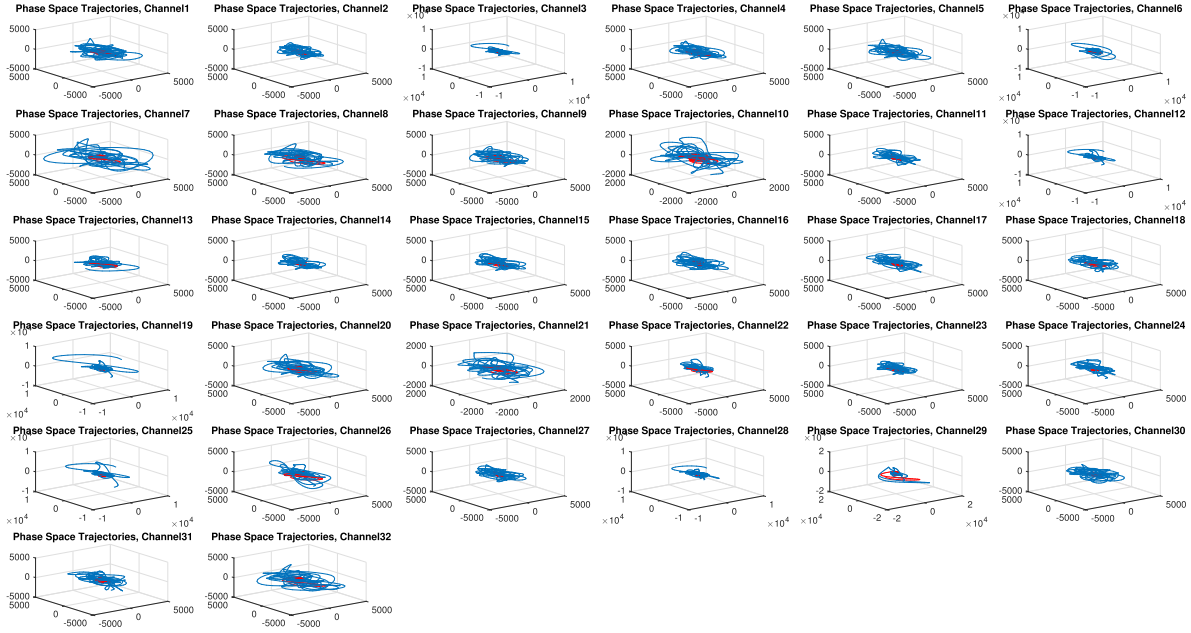

FIGURE 6. Trajectory of the S13's EEG in the reconstructed phase space based on the CTWO method for the 32 channels. The Tug of War optimizer method achieved FNN = 82 and MI = 11. The blue line is the trajectory of the imaginary right hand fisting and the red line is the no imagination.

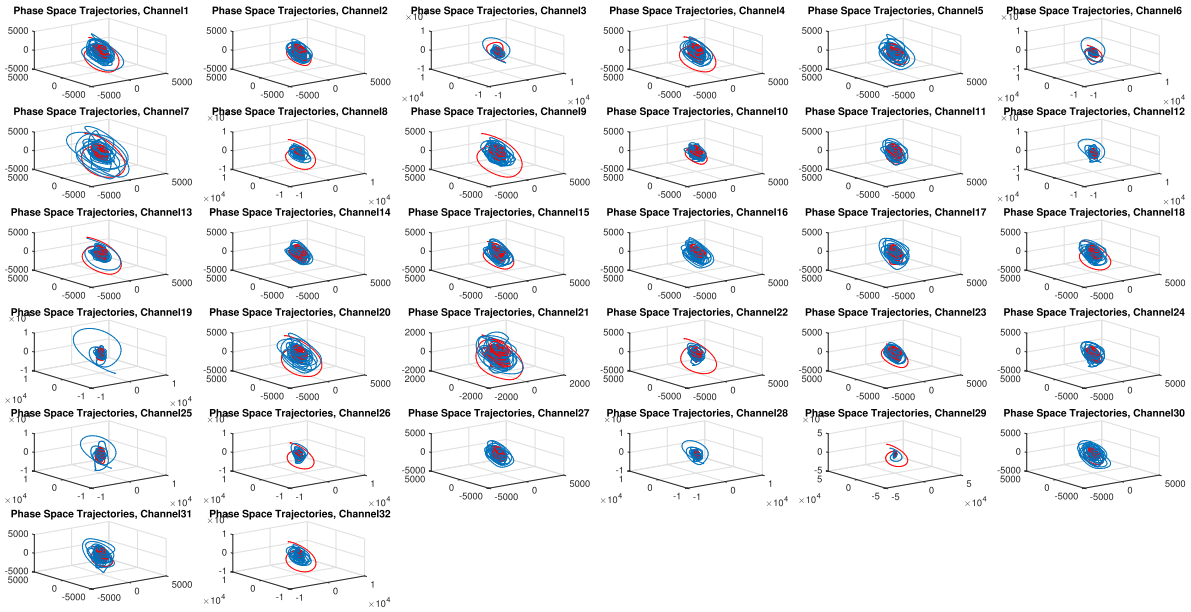

FIGURE 7. Trajectory of the S13's EEG in the reconstructed phase space based on the traditional method for the 32 channels. Based on the traditional method FNN = 3 and the MI = 5 are achieved. The blue line is the trajectory of the imaginary right hand fisting and the red line is the no imagination.

V. DISCUSSION

It is revealed that the Chaos Theory is helpful for the EEG signal processing interpretation and analyzing. One prominent chaos-based feature is the LLE. To compute the LLE, first a phase space is reconstructed and trajectory of the EEG is then grew in the phase space. Regarding the Taken's Theory [24] a phase space is reconstruct able by specifying appropriate embedding dimension and time lag. For this purpose, a time lag and an embedding dimension are specified through MI and FNN approaches, respectively. In this study,

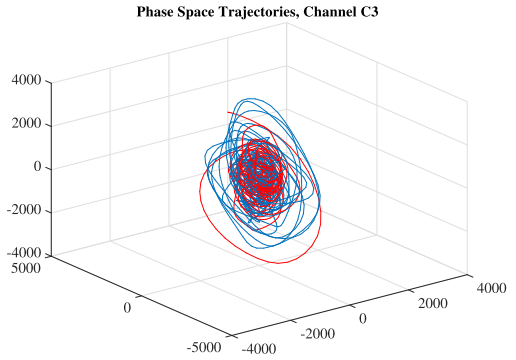

(a) Trajectory of the S13's EEG in the reconstructed phase space based on the traditional method (FNN=3 and MI=5 parameters) for the C3 channel.

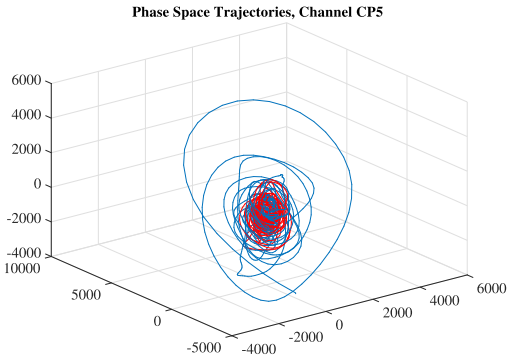

(b) Trajectory of the S13's EEG in the reconstructed phase space based on the traditional method (FNN=3 and MI=5 parameters) for the CP5 channel.

FIGURE 8. Trajectory of the EEG in the reconstructed phase space based on the traditional method for the C3 and CP5 channels.

an approximation method is utilized to obtain the optimum values for the FNN the MI approaches to reconstruct a phase space and classifying the extracted CALLE features.

The Tug of War optimization algorithm works on the definition in a competitive league. In the algorithm, each candidate solution is supposed as one of the teams in the league. The update formula of candidates is developed based on the qualities of the teams, which are interacted with each other. The basic algorithm, uses stochastic updating formula to find better solutions. In order to improve its performance, a new version named CTWO is investigated, which utilizes chaotic maps instead of stochastic approach. The chaotic maps is applied on the approach because of non-repeating and ergodicity behavior.

Based on the approximated values for the FNN and MI, features are extracted from the most informative channels and frequency bands. Demonstrated Fig. 5 gives overall information of the EEG trajectories in different locations and helped for finding the right channels for further computations. Regarding our previous experiment, the C3 and CP5 channels among the 32 channels are the most informative locations for identifying the imaginary movement patterns; and the

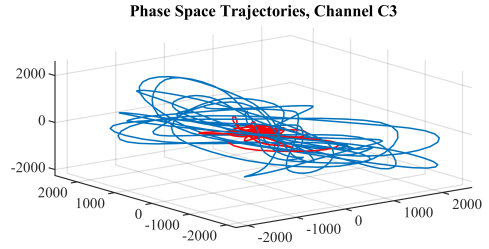

(a) Trajectory of the S13's EEG in the reconstructed phase space based on the CTWO method for the C3 channel (FNN=82 and MI=11 parameters).

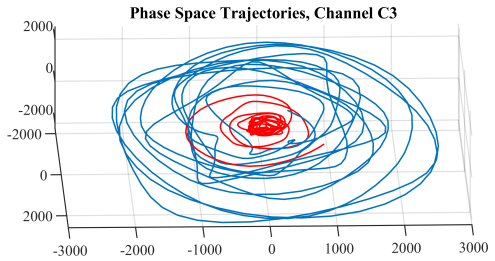

(b) Trajectory of the S13's EEG in the reconstructed phase space based on the CTWO method for the C3 channel (FNN=82 and MI=11 parameters).

FIGURE 9. Changing the trajectory projection of the EEG in the reconstructed phase space for the channel C3.

8-13 Hz frequency band is determined as the most informative frequency range for detecting the imaginary movement patterns [3]. Regarding the Taken's theory [24], two parameters of a time lag and an embedding dimension are required for reconstructing the phase space. Traditionally, the time lag and embedding dimension are computed based on the MI and FNN methods, respectively. The criterion for the maximum time lag ($\tau = 10$) in the MI and maximum embedding dimension ($n = 3$) in the FNN are determined experimentally. Also, methods are utilized to predict the best value for the maximum lag such as Fraser and Swinney methods [35]. The MI approach was utilized to exploit data between two interval samples with τ lag. More specifically, in the MI computations, two inputs of the segmented EEG signal and maximum time lag are required, in which the lag is a constant value and computed by Fraser and Swinney methods [35]. The second parameter in the Taken's theory is the FNN approach, which is utilized for specifying the embedding space dimension. More specifically, the FNN is also required two parameters, which are the segmented EEG signal and maximum embedding dimension. The maximum embedding dimension is a constant value and estimated by different methods [25], [36], [37]. Afterward, two phase spaces are reconstructed based on the traditional and approximated FNN and MI for growing the trajectories of the EEG data. The CALLE and LLE features are then extracted separately. In summary, four free parameters are defined at the same time to estimate the FNN and MI values for imaginary right-hand fisting and no fisting status. The CTWO approach was trained for 100 times and the average values of the maximum embedding

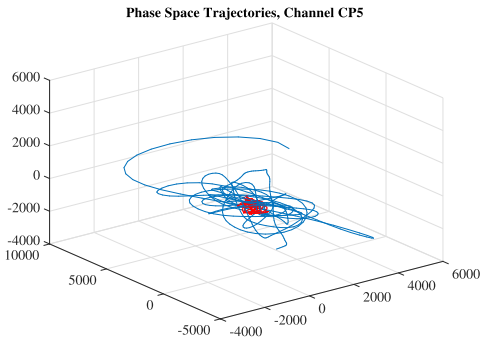

(a) Trajectory of the S13's EEG in the reconstructed phase space based on CTWO method for the CP5 channel (FNN=82 and the MI=11 parameters).

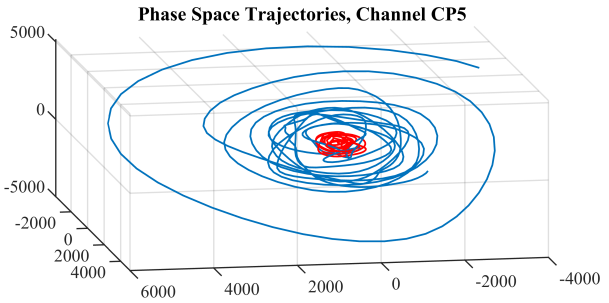

(b) Trajectory of the S13's EEG in the reconstructed phase space based on the CTWO method for the CP5 method from different projection (FNN=82 and the MI=11 parameters).

FIGURE 10. Changing the trajectory projection of the EEG in the reconstructed phase space for channel CP5.

dimensions and maximum time lags are utilized and presented in Table 4. The CTWO, specified different sets of solutions to reach the same reported accuracy values in Table 4.

Regarding Figs 8a, 8b and 7, it is revealed that the trajectories in the phase space based on the traditional MI and FNN are highly mixed that the obtained average accuracy of the identifying imaginary patterns is similar to random (average accuracy 57.77%), Table 5. Regarding Table 5, the computed MIs and FNNs based on the traditional approaches for the fisting imaginary state are between 5 to 30 (mostly close to 5) and 1.94 to 2 (mostly close to 2), respectively. Although, Table 4 shows that the MIs and FNNs based on the CTWO for the same imaginary movement state are obtained different values between 2 to 70 and 6 to 47, respectively. Also, Regarding Table 5, the computed traditional MIs and FNNs for no imaginary movement are the same as the imaginary movement. Although, Table 4 shows that the MIs and FNNs for the no imaginary movement are obtained different values between 5 to 81 and 2 to 48, respectively. By investigating Figs. 6, 9 and 10, meaningful enhancement for the two obtained state trajectories in the channels C3 and CP5 are seen, respectively. More specifically, Figs. 9a and 10a shows that no fisting imagination's trajectories are centered at the middle of the hand fisting imagination trajectories. By changing the Figs'. 9b and 10b projections separability of the trajectories for the two classes is recognizable and results are improved consequently, Table 4. The LLE values and Figs. 9a and 10 shows that at the moment of the imagination, the EEG tends to have chaotic behavior (blue lines) and thereafter the EEG behavior back to previous state (red lines). The extracted CALLE and traditional LLE features are then classified status using the SMSVM classifier with the GRBF kernel separately.

The obtained average accuracies in Tables 4 and 5 shows that the estimated MI and FNN reconstructed a better phase space and attained higher average accuracy of 67.60%. The presented results shows 9.83% higher accuracy in comparison with the traditional method. In order to consider the meaningfulness of the feature changes between the two status, statistical analysis paired t-test for individual subjects is employed. Tables 4 and 5 shows that one subject's paired t-test for the CALLE changes were not significant ($P > 0.05$), 17 subjects' paired t-test were significant ($P < 0.05$), while the seven subjects for the traditional LLE changes were not significant ($P > 0.05$). A trained algorithm of the SMSVM classifier is utilized for controlling a bionic hand in the real-time mode that the results were not reliable enough and needs more de-noising computations to have better EEG signals and results.

VI. CONCLUSION

LLE is a successful chaotic method for the EEG pattern recognition. In the presented approach, the traditional LLE has been approximated utilizing the CTWO method. In the procedure, the EEG signals based on imaginary fisting movements are recorded, filtered and segmented. The best values for the FNN and MI have been computed based on the traditional and chaotic Tug of War optimization methods for reconstructing a phase space. The new developed algorithm has been employed the chaotic maps to update the candidate solution. The proposed algorithm has been applied on benchmark functions and results are compared with traditional methods. Achieved accuracy results and obtained figures have depicted significant enhancement for the CALLE in comparison with the traditional LLE. The averaged results based on the CALLE has reached to 68.25% with 17 significant $P-$vales among 18 subjects. Also, it has been achieved that the optimum values of the FNN and MI to reach the best accuracy are not unique.

REFERENCES

[1] A. Hekmatmanesh, F. Jamaloo, H. Wu, H. Handroos, and A. Kilpeläinen, "Common spatial pattern combined with Kernel linear discriminate and generalized radial basis function for motor imagery-based brain computer interface applications," in *Proc. AIP Conf.*, 2018, vol. 1956, no. 1, Art. no. 020003.

[2] K. K. Ang, Z. Y. Chin, H. Zhang, and C. Guan, "Filter bank common spatial pattern (FBCSP) in brain-computer interface," in *Proc. IEEE Int. Joint Conf. Neural Netw. (IEEE World Congr. Comput. Intell.)*, Jun. 2008, pp. 2390–2397.

[3] A. Hekmatmanesh, H. Wu, M. Li, A. M. Nasrabadi, and H. Handroos, "Optimized mother wavelet in a combination of wavelet packet with detrended fluctuation analysis for controlling a remote vehicle with imagery movement: A brain computer interface study," in *New Trends in Medical and Service Robotics*. Cham, Switzerland: Springer, 2019, pp. 186–195.

[4] A. Hekmatmanesh, H. Wu, A. Motie-Nasrabadi, M. Li, and H. Handroos, "Combination of discrete wavelet packet transform with detrended fluctuation analysis using customized mother wavelet with the aim of an imagery-motor control interface for an exoskeleton," in *Multimedia Tools and Applications*. New York, NY, USA: Springer, 2019, pp. 1–20.
[5] S. M. R. Noori, A. Hekmatmanesh, M. Mikaeili, and K. Sadeghniiat-Haghighi, "K-complex identification in sleep EEG using MELM-GRBF classifier," in *Proc. 21th Iranian Conf. Biomed. Eng. (ICBME)*, Nov. 2014, pp. 119–123.
[6] A. Hekmatmanesh, S. M. R. Noori, and M. Mikaili, "Sleep spindle detection using modified extreme learning machine generalized radial basis function method," in *Proc. 22nd Iranian Conf. Elect. Eng. (ICEE)*, May 2014, pp. 1898–1902.
[7] S. Vaid, P. Singh, and C. Kaur, "EEG signal analysis for BCI interface: A review," in *Proc. 5th Int. Conf. Adv. Comput. Commun. Technol.*, Feb. 2015, pp. 143–147.
[8] A. Hekmatmanesh, M. Mikaeili, K. Sadeghniiat-Haghighi, H. Wu, H. Handroos, R. Martinek, H. Nazeran, "Sleep spindle detection and prediction using a mixture of time series and chaotic features," *Adv. Elect. Electron. Eng.*, vol. 15, no. 3, pp. 435–447, 2017.
[9] J. E. Jacob, V. V. Sreelatha, T. Iype, G. K. Nair, and D. G. Yohannan, "Diagnosis of epilepsy from interictal EEGs based on chaotic and wavelet transformation," *Analog Integr. Circuits Signal Process.*, vol. 89, pp. 131–138, Oct. 2016.
[10] M. R. Mohammadi, A. Khaleghi, A. M. Nasrabadi, S. Rafieivand, M. Begol, and H. Zarafshan, "EEG classification of ADHD and normal children using non-linear features and neural network," *Biomed. Eng. Lett.*, vol. 6, no. 2, pp. 66–73, 2016.
[11] A. Allahverdy, A. K. Moghadam, M. R. Mohammadi, and A. M. Nasrabadi, "Detecting ADHD children using the attention continuity as nonlinear feature of EEG," *Frontiers Biomed. Technol.*, vol. 3, nos. 1–2, pp. 28–33, 2017.
[12] A. I. Korda, P. A. Asvestas, G. K. Matsopoulos, E. M. Ventouras, and N. Smyrnis, "Automatic identification of eye movements using the largest Lyapunov exponent," *Biomed. Signal Process. Control*, vol. 41, pp. 10–20, Mar. 2018.
[13] P. Dahal, T. Ning, and J. H. Blaise, "Chaotic analysis of hippocampal and cortical sleep EEG during various vigilance states," in *Proc. 40th Annu. Int. Conf. IEEE Eng. Med. Biol. Soc. (EMBC)*, Jul. 2018, pp. 3064–3067.
[14] R. M. Asl, F. Hashemzadeh, and M. A. Badamchizadeh, "A new adaptive neural network based observer for robotic manipulators," in *Proc. 3rd RSI Int. Conf. Robot. Mechatronics (ICROM)*, Oct. 2015, pp. 663–668.
[15] R. M. Asl, A. Mahdoudi, E. Pourabdollah, and G. Klančar, "Combined PID and LQR controller using optimized fuzzy rules," *Soft Comput.*, vol. 23, pp. 5143–5155, Jul. 2019.
[16] M. S. Nobarian, R. M. Asl, M. Nemati, and F. Hashemzadeh, "Optimal L1 control for linear time-delayed systems using GSA algorithm," in *Proc. 4th Int. Conf. Control, Instrum. Automat. (ICCIA)*, Jan. 2016, pp. 111–115.
[17] T. Nguyen, A. Khosravi, D. Creighton, and S. Nahavandi, "EEG signal classification for BCI applications by wavelets and interval type-2 fuzzy logic systems," *Expert Syst. Appl.*, vol. 42, no. 9, pp. 4370–4380, Jun. 2015.
[18] M. G. Doborjeh, G. Y. Wang, N. K. Kasabov, R. Kydd, and B. Russell, "A spiking neural network methodology and system for learning and comparative analysis of EEG data from healthy versus addiction treated versus addiction not treated subjects," *IEEE Trans. Biomed. Eng.*, vol. 63, no. 9, pp. 1830–1841, Sep. 2016.
[19] R. M. Asl, E. Pourabdollah, and M. Salmani, "Optimal fractional order PID for a robotic manipulator using colliding bodies design," *Soft Comput.*, vol. 22, no. 14, pp. 4647–4659, 2018.
[20] X. Tang, N. Zhang, J. Zhou, and Q. Liu, "Hidden-layer visible deep stacking network optimized by PSO for motor imagery EEG recognition," *Neurocomputing*, vol. 234, pp. 1–10, Apr. 2017.
[21] D. Rodrigues, G. F. A. Silva, J. P. Papa, A. N. Marana, and X.-S. Yang, "EEG-based person identification through binary flower pollination algorithm," *Expert Syst. Appl.*, vol. 62, pp. 81–90, Nov. 2016.
[22] A. Kaveh, "Tug of war optimization," in *Advances in Metaheuristic Algorithms for Optimal Design of Structures*. Cham, Switzerland: Springer, 2017, pp. 451–487.
[23] A. Kaveh, "Optimum design of castellated beams using the tug of war algorithm," in *Applications Metaheuristic Optimization Algorithms in Civil Engineering*. Cham, Switzerland: Springer, 2017, pp. 9–30.
[24] L. Noakes, "The Takens embedding theorem," *Int. J. Bifurcation Chaos*, vol. 1, no. 4, pp. 867–872, 1991.
[25] M. B. Kennel, R. Brown, and H. D. I. Abarbanel, "Determining embedding dimension for phase-space reconstruction using a geometrical construction," *Phys. Rev. A, Gen. Phys.*, vol. 45, no. 6, p. 3403, Mar. 1992.
[26] M. T. Rosenstein, J. J. Collins, and C. J. De Luca, "A practical method for calculating largest Lyapunov exponents from small data sets," *Phys. D, Nonlinear Phenomena*, vol. 65, pp. 117–134, May 1993.
[27] H. Kantz, "A robust method to estimate the maximal Lyapunov exponent of a time series," *Phys. Lett. A*, vol. 185, no. 1, pp. 77–87, Jan. 1994.
[28] A. Kaveh and A. Zolghadr, "A novel meta-heuristic algorithm: Tug of war optimization," *Iran Univ. Sci. Technol.*, vol. 6, no. 4, pp. 469–492, 2016.
[29] S. Saremi, S. Mirjalili, and A. Lewis, "Biogeography-based optimisation with chaos," *Neural Comput. Appl.*, vol. 25, no. 5, pp. 1077–1097, 2014.
[30] A. H. Gandomi, X.-S. Yang, S. Talatahari, and A. H. Alavi, "Firefly algorithm with chaos," *Commun. Nonlinear Sci. Numer. Simul.*, vol. 18, no. 1, pp. 89–98, Jan. 2013.
[31] G. Kaur and S. Arora, "Chaotic whale optimization algorithm," *J. Comput. Des. Eng.*, vol. 5, no. 3, pp. 275–284, 2018.
[32] F. Fernández-Navarro, C. Hervás-Martínez, J. Sanchez-Monedero, and P. A. Gutiérrez, "MELM-GRBF: A modified version of the extreme learning machine for generalized radial basis function neural networks," *Neurocomputing*, vol. 74, no. 16, pp. 2502–2510, 2011.
[33] C.-C. Chang and C.-J. Lin, "LIBSVM: A library for support vector machines," *ACM Trans. Intell. Syst. Technol.*, vol. 2, no. 3, pp. 27:1–27:27, 2011.
[34] J. A. K. Suykens and J. Vandewalle, "Least squares support vector machine classifiers," *Neural Process. Lett.*, vol. 9, no. 3, pp. 293–300, Jun. 1999.
[35] A. M. Fraser and H. L. Swinney, "Independent coordinates for strange attractors from mutual information," *Phys. Rev. A, Gen. Phys.*, vol. 33, no. 2, p. 1134, 1986.
[36] D. Chelidze, "Reliable estimation of minimum embedding dimension through statistical analysis of nearest neighbors," *J. Comput. Nonlinear Dyn.*, vol. 12, no. 5, 2017, Art. no. 051024.
[37] L. Zhao, L. Wang, Y. Wang, Z. Huang, and N. Fang, "Determining minimum embedding dimension in short time series using precisely averaged false-nearest-neighbors approach," in *Proc. China-Japan Joint Microw. Conf.*, Sep. 2008, pp. 554–557.

AMIN HEKMATMANESH received the bachelor's degree in electrical engineering from the Islamic Azad University, Science and Research of Fars, Shiraz, Iran, in 2010, and the master's degree in biomedical engineering from Shahed University, Tehran, Iran, in 2013. His master's thesis was on analyzing sleep EEG signal processing, learning and negative emotional memory. Since 2016, he has been a Researcher with the Laboratory of Intelligent Machines, Lappeenranta University of Technology, Finland. His current research interest includes brain-controlled ankle foot orthosis robot.

REZA MOHAMMADI ASL received the B.Sc. and M.Sc. degrees in electrical engineering and control systems from the University of Tabriz, Tabriz, Iran, in 2013 and 2015, respectively. He is currently a Junior Researcher with LUT University, Finland. His current research interests include nonlinear control, artificial intelligence, robotics, and hydraulic systems.

HUAPENG WU was born in Wuhan, China, in 1964. He received Doctor of Science (Tech.) degree from the Lappeenranta University of Technology, Finland, in 2001. Since 2004, he has been an Associate Professor with the Lappeenranta University of Technology, where he was a Professor, from 2008 to 2011. His research interests include robotics, AI control, mechatronics, mechanical manufacturing, and automation. He has published four books and more than 100 publications in his research areas.

HEIKKI HANDROOS received the M.Sc. (Eng.) and D.Sc. (Tech.) degrees from the Tampere University of Technology, in 1985 and 1991, respectively. He has been a Professor of machine automation with the Lappeenranta University of Technology, since 1992. He has been a Visiting Professor with the University of Minnesota, the Peter the Great St. Petersburg Polytechnic University, and the National Defense Academy, Japan. He has led several important domestic and international research projects. He has published about 300 international scientific papers and supervised around 20 D.Sc. (Tech.) theses. His research interests include modeling, design, and control of mechatronic transmissions to robotics and virtual engineering. He has been an Associate Editor of the *Journal of Dynamic Systems, Measurement, and Control* (ASME), since 2014.